Climate Dynamics (2024) 62:3189–3206
https://doi.org/10.1007/s00382-023-07058-1

ORIGINAL ARTICLE

New insights on ENSO teleconnection asymmetry and ENSO forced atmospheric circulation variability over North America

Margaret Sutton[1] · Sarah M. Larson[1] · Emily Becker[2]

Received: 7 February 2023 / Accepted: 4 December 2023 / Published online: 10 January 2024

Abstract

El Niño-Southern Oscillation (ENSO)-related sea surface temperature variability in the eastern equatorial Pacific drives an extratropical large-scale atmospheric response. The atmospheric response is a key driver of global climate variability, with the strongest impact occurring during Northern Hemisphere winter. The degree to which atmospheric circulation variability is altered during ENSO events, in comparison with atmospheric circulation variability during ENSO-neutral conditions, is the focus of this study. Two multi-century, CESM1-CAM4 simulations are compared: a fully coupled experiment (CTRL), and a partially decoupled experiment in which ENSO is dynamically suppressed (NoENSO) so that the mean state is not biased towards a particular ENSO phase. We present evidence that the rectification of ENSO and its teleconnections onto the mean state lead to an underestimation of the asymmetry of ENSO teleconnections in this model. Analyses also show that ENSO displaces 500 hPa geopotential height (Z500) variability away from the central northern U.S. and southern Canada, resulting in less variability during ENSO years than ENSO-neutral years. Additionally, we find that estimating the ENSO-forced change in Z500 variance compared to ENSO-neutral years requires a surprisingly large sample of ENSO-neutral years. The results imply that a substantially longer record–roughly an order of magnitude longer in length–is needed to fully capture the statistics of ENSO's teleconnected impacts over North America than suggested in previous studies.

Keywords ENSO impacts · ENSO teleconnections · Seasonal climate · North American climate · Climate modeling

1 Introduction

El Niño-Southern Oscillation (ENSO), or the fluctuation of sea surface temperature (SST) in the equatorial Pacific Ocean, is the dominant source of interannual atmospheric circulation and terrestrial climate predictability over North America (Ropelewski and Halpert 1986, 1987). The connection between local ENSO forcing in the tropical Pacific and climatic impacts in the extratropics are often referred to as ENSO teleconnections and can be explained by tropical and extratropical atmospheric dynamics (Gill 1980; Hoskins and Karoly 1981). ENSO-forced precipitation anomalies drive divergence and vorticity anomalies in the upper atmosphere of the tropical Pacific, exciting a stationary Rossby wave train pattern into the midlatitudes (Hoskins and Karoly 1981; Sardeshmukh and Hoskins 1988). The resulting shift in the large-scale atmospheric circulation alters global weather patterns, which can enhance the risk of natural disasters, such as droughts, heavy rainfall, floods, and heat waves (Ropelewski and Halpert 1987; Dilley and Heyman 1995). These terrestrial impacts can influence the severity of ecological and economical disasters, such as the destruction of fisheries, low crop yield, and water scarcity (McPhaden et al. 2006). However, predicting the ENSO signal has proven difficult due to the abundance of other sources of internal variability, which act as noise and can cloud the ENSO signal (Kumar and Chen 2017; Deser et al. 2018).

The ENSO-forced Rossby wave train in the Northern Hemisphere projects onto an anomalous atmospheric circulation pattern that resembles the Pacific North American pattern (PNA; Wallace and Gutzler 1981)). Put simply, the PNA is the resulting spatial pattern of atmospheric variability associated with changes in the Pacific jet (Hoerling et al. 1997). The phase of the PNA is often linked to the phase of ENSO (Hoerling and Kumar 2002), hence the precipitation

✉ Margaret Sutton
slarson@ncsu.edu

[1] Department of Marine, Earth, and Atmospheric Sciences, North Carolina State University, Raleigh, NC, USA

[2] Cooperative Institute for Marine and Atmospheric Studies, University of Miami, Miami, FL, USA

and surface temperature impacts over North America associated with the PNA are often considered similar to those associated with ENSO (Ropelewski and Halpert 1987; Harrison and Larkin 1998). For example, during an El Niño event, the Aleutian low is anomalously deep, anomalous ridging occurs over northwest North America, and anomalous troughing occurs over the southeast U.S., thus projecting onto the positive PNA pattern. Wetter-than-average conditions over the southern U.S. and drier conditions over the northeast and northwest U.S. usually accompany this pattern. The opposite patterns occur for La Niña and the negative PNA. Yet not every El Niño or La Niña event results in these canonical patterns, due to other naturally occurring large-scale atmospheric patterns that can impact North American precipitation (L'Heureux et al. 2017; Peng et al. 2018, 2019). There is also evidence that the ENSO-forced atmospheric circulation response exhibits important distinctions from the typical PNA pattern (Livezey and Mo 1987; Trenberth et al. 1998; Hoerling and Kumar 2002; Straus and Shukla 2002; Johnson and Feldstein 2010; Li et al. 2019) that result in significant differences in winter precipitation signatures across the southeastern U.S. (Larson et al. 2022). Therefore, robustly characterizing ENSO's impact on atmospheric circulation variability, or variance, is critical to determine the predictability of seasonal climate anomalies over North America. To do so, it is first necessary to characterize and compare the amplitude of non-ENSO variations (i.e., the "noise") to those related to ENSO (i.e., the "signal"), which is an important goal of our study.

Isolating and removing the ENSO signal and its related teleconnections, so as to estimate the non-ENSO variance, is commonly accomplished through statistical approaches summarized in Compo and Sardeshmukh (2010). One method is to bandpass filter SST to remove the interannual variations, thus assuming only and all variability within the defined frequency band is related to ENSO. However, ENSO and its teleconnections are known to have a low frequency signal (Wittenberg et al. 2014). Another method is to linearly "regress out" the ENSO signal through computing the linear regression of climate variables onto an ENSO time series, like Niño3.4, and subsequently remove the linear ENSO contribution from the anomaly fields. This approach assumes all variations captured by the ENSO time series are strictly ENSO related, which is not necessarily true (e.g., see thermally coupled modes in Larson et al. 2018a, b), and lagged responses to ENSO (Su et al. 2005) are nearly impossible to fully remove. This approach is further complicated by the issue that ENSO variations are tightly linked to the seasonal cycle (Stuecker et al. 2013). Furthermore, ENSO itself and its teleconnections exhibit marked nonlinearities (e.g., Frauen et al. 2014) that are neglected in linear approaches. More sophisticated modeling approaches have also aimed to compare ENSO and non-ENSO variations. One method is through the Linear Inverse Modeling (LIM) framework, in which atmospheric variations can be identified as coupled or uncoupled to the tropical SST (Newman et al. 2009). Through removing atmospheric modes coupled to tropical SST, Henderson et al. (2020) investigate PNA growth related and unrelated to tropical SST. One caveat to this approach related to our purposes is atmospheric variability forced by non-ENSO tropical SST may be excluded, thus potentially underestimating non-ENSO atmospheric variance. For similar reasons, tropical pacemaker simulations in which the tropical Pacific SST is prescribed as climatology may also underestimate non-ENSO atmospheric variability originating from the tropical Pacific, as well as shut off non-ENSO tropical-to-extratropical ocean pathways that may drive midlatitude variability. Finally, compositing and comparing atmospheric patterns during ENSO-neutral versus ENSO years can be useful, but the observational record is limited and other sources of natural variability can overshadow the ENSO signal (e.g., Deser et al. 2018).

Recently, a coupled model method that dynamically suppresses ENSO variability has proven effective in removing both ENSO and its teleconnected impacts without the aforementioned caveats. In this method, the equatorial Pacific Ocean is unable to dynamically respond to anomalous wind stress variability, thereby breaking the Bjerknes feedback (Bjerknes 1969), the coupled wind-ocean feedback required for ENSO growth (as demonstrated in Larson and Kirtman 2015; Larson et al. 2018b). The result is a simulation of Earth's climate devoid of ENSO variability but inclusive of all other variations resolved by the model. We hereafter refer to this as a "NoENSO" experiment. By comparing the impacts of PNA variability in a control version of the coupled model that includes ENSO variability and a "NoENSO" version of the same model, Larson et al. (2022) demonstrate that this approach facilitates clean comparison of ENSO-forced and non-ENSO-forced extratropical climate variations. Furthermore, the reference climatology from the NoENSO simulation can be used as an unbiased estimate of the ENSO-neutral state from which to compute ENSO-related climate anomalies in the control run.

The purpose of this study is to investigate ENSO-driven impacts on interannual mid-level atmospheric circulation variability by comparing a world with ENSO to a world without ENSO. We accomplish this through the comparison of novel climate model experiments that cleanly separate ENSO and non-ENSO variability. We address science questions such as the following: To what extent do asymmetries related to ENSO and/or its teleconnections bias the mean state and impact interpretations of the asymmetry of ENSO teleconnections? How does ENSO alter mid-level atmospheric circulation variability over North America? How long of a simulation length is needed to resolve the ENSO forced change in mid-level atmospheric circulation variability?

Model experiments are introduced in Sect. 2. Analysis and comparison of these simulations in Sects. 3.1 and 3.2 demonstrate how ENSO composites, when constructed using an ENSO biased mean state as the reference climatology for computing anomalies, can underestimate the asymmetry of ENSO teleconnections. Sections 3.3–3.4 analyze the ENSO versus non-ENSO contributions to atmospheric circulation variability and include a model-derived estimate of how many ENSO neutral years are required to resolve the ENSO forced variance, the results of which are subsequently tested in Sect. 3.5 using a different model. Summary and conclusions are provided in Sect. 4.

2 Data and Methods

2.1 Observational and Reanalysis Datasets

The observed SST dataset used is the Extended Reconstruction Sea Surface Temperature version 5 (ERSSTv5; Huang et al. 2017). The horizontal grid spacing of the ERSSTv5 is $2° \times 2°$. All calculations in this study use the full time series from 1950–2020. SST data is available prior to 1950, but is less reliable (Huang et al. 2017).

Reanalysis products are used to analyze 500 hPa geopotential heights (Z500), which we use to represent mid-level atmospheric circulation and its variability. The first dataset is from the National Centers for Environmental Prediction (NCEP)-National Center for Atmospheric Research (NCAR) reanalysis project (hereafter, NCEP/NCAR reanalysis; Kalnay et al. 1996). The NCEP/NCAR reanalysis dataset is available from 1948-present on a $2.5° \times 2.5°$ horizontal grid. The second reanalysis product used is the European Centre for Medium-Range Weather Forecasts reanalysis version 5 (hereafter, ERA5 reanalysis; Hersbach et al. 2020). The ERA5 reanalysis dataset is available from 1950-present with approximately a $0.25° \times 0.25°$ horizontal resolution. All analyses from observations and reanalyses are from the time period 1950–2020.

2.2 Model experiments

2.2.1 CESM1-CAM4 Control (CTRL)

The first model used in this study is the Community Earth System Model version 1 coupled to the Community Atmospheric Model version 4 (CESM1-CAM4, Worley et al. 2011). CESM1-CAM4 has a nominal horizontal resolution of 1° and is forced with a constant radiative forcing from the year 2000 (i.e., "present day"). The Parallel Ocean Program version 2 (POP2; Smith et al. 2010) is the ocean component in CESM1-CAM4. The atmospheric component is CAM4 (Neale et al. 2013), which is different from the out-of-the-box version of CESM1 that includes the updated CAM5. For this reason, CESM1-CAM4 compares closely to Community Climate System Model version 4 (CCSM4; Gent et al. 2011), however with updated diabatic processes parameterizations found in the typical CESM1 (Hurrell et al. 2013). CCSM4 produces a realistic ENSO-related spatial pattern and frequency, as well as ENSO teleconnections (Deser et al. 2012). The control version of this model, hereafter "CTRL," is the typical fully coupled version that includes ENSO variability. A total of 321 simulation years are available from the CTRL.

2.2.2 CESM1-CAM4 NoENSO Experiment

We analyze a second CESM1-CAM4 experiment in which ENSO variability is eliminated through the suppression of the dynamical processes that support ENSO variability, hereafter the "NoENSO" experiment (see also Larson et al. 2022; McMonigal and Larson 2022). The NoENSO experiment is performed using the same CESM1-CAM4 base model as the CTRL and is the same experiment analyzed in Larson et al. (2022) (named "MD_{EqPac}" in their study) to study PNA variations and precipitation impacts unrelated to ENSO. In the NoENSO experiment, the wind stress forcing on the tropical Pacific Ocean is prescribed as the seasonally varying daily wind stress climatology, thereby mechanically decoupling the ocean from the atmosphere. The wind stress climatology is computed from a 30-yr period of daily wind stress from the CTRL run that is representative of the climatology of the greater 321-yr period across the equatorial Pacific (not shown). This method of prescribing the wind stress does not alter the atmospheric turbulent heat flux formulation, as wind variability is still applied to the bulk formula. Therefore, while the anomalous wind stress is decoupled from the tropical Pacific Ocean, anomalous buoyancy fluxes remain unaltered, leaving the model thermodynamically coupled even in the tropical Pacific. By removing the atmosphere's ability to reinforce the initial SST anomaly through wind driven changes in the ocean dynamics, the Bjerknes feedback is deactivated, and ENSO events cannot develop. In this study, wind stress climatology is only prescribed along the equatorial Pacific basin (10°N-10°S, 120°E-60°W), with a linear tapering at the latitudinal boundaries (see Larson et al. 2022 for more details). Outside of this region, the CTRL and NoENSO experiments behave similarly with fully coupled, interactive atmosphere and ocean dynamics. The two experiments, CTRL and NoENSO, will be compared through a series of statistical analyses in this study. A total of 306 simulation years are available from the NoENSO experiment.

2.2.3 CESM2

The second model is the Community Earth System Model version 2 (CESM2; Danabasoglu et al. 2020). Similar to CESM1-CAM4, the horizontal grid spacing of CESM2 is approximately 1°. The atmospheric model is the Community Atmospheric Model version 6 (CAM6; Bogenschutz et al. 2018) with 32 vertical levels. CESM2 uses the same ocean model, POP2, as used in CESM1-CAM4. However, POP2 has been updated since CESM1 (Danabasoglu et al. 2020). CESM2 simulates realistic ENSO variability as well as ENSO teleconnections (Capotondi et al. 2020). This fully coupled simulation is the same CESM2 pre-industrial simulation contributed to the CMIP6 project (Eyring et al. 2016) and includes 2000 model years. In Sect. 3.4, we estimate the minimum number of ENSO neutral model years necessary to estimate ENSO's forced impact on Z500 variance. The CESM2 model is then used in Sect. 3.5 to test the estimate, given the abundance of model years available.

2.3 Analysis methods

To compare to variability in the two models, all observational and reanalysis datasets are linearly detrended to approximately remove the presence of anthropogenic trends. Generally, monthly anomalies are calculated by removing the respective monthly mean climatology of each experiment. Analyses in Sect. 3.2 will test the sensitivity of results when instead using the NoENSO reference climatology to compute ENSO composite anomalies in the CTRL. After calculating the monthly anomalies, seasonal averages are calculated using a three-month moving average. In this study, we focus on the boreal winter seasonal average (December-February, or DJF), given the largest ENSO-related anomalies in the equatorial Pacific and the most robust global teleconnected response to ENSO occur during these months.

To define ENSO events, the DJF SST anomalies in the equatorial Pacific are first area-weighted and averaged over the Niño3.4 region from 5°N-5°S, 120°-170°W. An El Niño event is defined as when the DJF Niño3.4 meets or exceeds 0.5 °C, whereas a La Niña event is defined when the DJF Niño3.4 is less than or equal to -0.5 °C. ENSO-neutral years are defined as when the magnitude of DJF Niño3.4 value is less than 0.5 °C.

The interannual variance is calculated using the DJF seasonal anomalies; this is done to show the amount of variability present from year-to-year during the boreal winter. To quantitatively examine ENSO's impact on interannual variability, the percent difference between the CTRL and NoENSO is examined throughout this study to investigate how the addition of ENSO's atmospheric forced response changes the overall variance, thus the variance difference is normalized by the NoENSO variance in the denominator. When the total DJF variances are directly compared between the experiments, we use a 306-yr sample from each experiment. In our analysis of observed fields, due to small sample sizes, the percent difference is computed as the variance difference between the ENSO versus ENSO-neutral winters, relative to the variance of the ENSO-neutral winters.

The NoENSO experiment contains very little variability in the Niño3.4 region, as Larson et al. (2022) report the standard deviation of Niño3.4 is roughly 0.16 °C. This indicates the Niño3.4 region in NoENSO remains close to climatology throughout the simulation. This 0.16 °C threshold will later be used to define ENSO-neutral years. However, a sufficient sample of ENSO-neutral years with such a closely climatological state, i.e., with a Niño-3.4 of $\pm$ 0.16 °C, is impossible to obtain from observations. Therefore, we follow the typical approach for defining ENSO-neutral in observations, as when the amplitude of the DJF Niño3.4 anomaly is less than 0.5 °C. An F-test is used to determine at what locations the difference in variance is statistically significantly different.

3 Results

3.1 ENSO variability

We first demonstrate the lack of ENSO variability in the NoENSO experiment. Figure 1 shows the DJF SST anomaly variance in the CTRL and NoENSO experiments. The CTRL shows large SST variability in the equatorial Pacific indicative of ENSO variability that is absent in NoENSO. NoENSO also shows weaker variance in the North Pacific where SST variability can be forced remotely via ENSO through the "atmospheric bridge" mechanism (Lau and Nath 1994; Alexander et al. 2002; Liu and Alexander 2007). Similar differences can be seen if the variance is instead computed from all months (see Larson et al. 2022 their Fig. 1b, c).

The DJF Niño3.4 index is used to depict 100 arbitrary year-to-year ENSO events in the CTRL (Fig. 2). The red horizontal lines show the 0.5 °C magnitude thresholds for ENSO events. For comparison, the blue lines show $\pm$ 0.16 °C, the Niño3.4 standard deviation from NoENSO, indicating the interannual SST variations in the NoENSO experiment fall well below the typical threshold for defining ENSO events. The removal of canonical ENSO is further confirmed by the power spectrum analysis of McMonigal and Larson 2022; see their Fig. 1a). Finally, given that anomalous deep convection in the tropical Pacific is the driving force for ENSO teleconnections, we show the percent difference in precipitation variance between the two experiments (Fig. 3). The CTRL

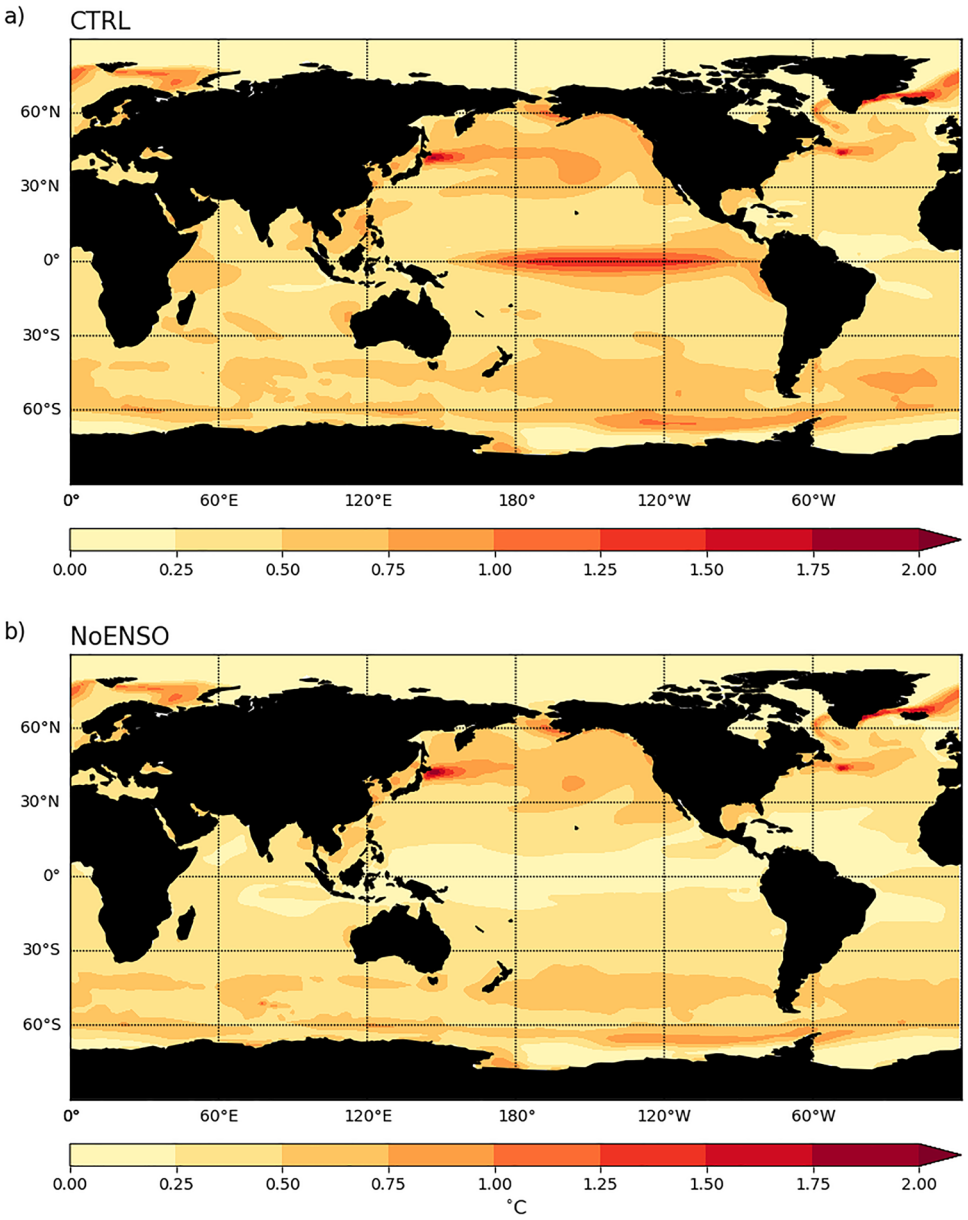

Fig. 1 DJF SST variance from CESM1-CAM4 **a** CTRL and **b** NoENSO experiments. Units are $(°C)^2$

simulates larger precipitation variability in the tropical Indo-Pacific compared to NoENSO, indicative of ENSO's role in modulating tropical precipitation.

Based on these multiple lines of evidence and further analyses of these experiments in Larson et al. (2022), we conclude that the NoENSO experiment indeed lacks canonical ENSO variability and remains close to climatology throughout the simulation. Larson et al. (2018a) show that the weak monthly Niño3.4 SST variability that occurs in the NoENSO experiment is thermodynamically forced from the extratropical South Pacific: this is non-ENSO tropical SST variability that could drive a weak extratropical teleconnection, thus should be included in estimates of non-ENSO variance. We also note that even though 0.5 °C is the typical threshold used to delineate ENSO-neutral and ENSO years, this threshold allows for considerably more tropical Pacific SST variability than occurs in the NoENSO experiment.

3.2 Impact of ENSO-biased mean state on ENSO teleconnection asymmetry

Figure 4 shows the difference between the CTRL and NoENSO DJF mean state for SST, Z500, sea level pressure (SLP), and precipitation. Compared to NoENSO, the CTRL SST is warmer in the eastern equatorial Pacific and cooler in the west, consistent with a weakening of the zonal SST gradient typical during El Niño. Since El Niño events in observations tend to be stronger (higher amplitude anomaly in Niño3.4) than La Niña events (e.g., An and Jin 2004), we initially suspected that this SST mean state difference and

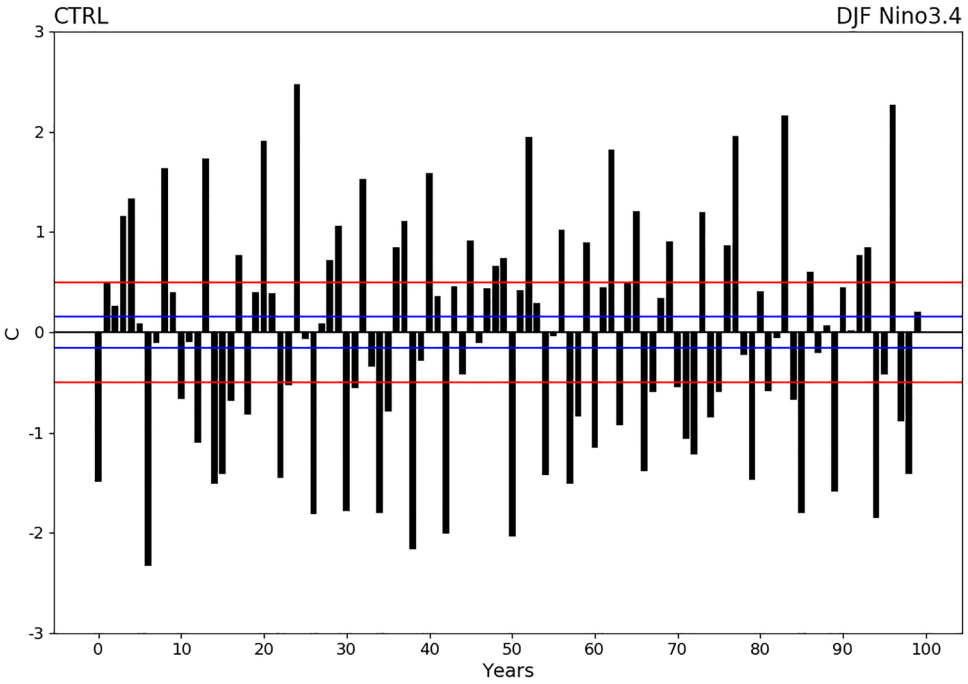

Fig. 2 DJF SST anomalies area-averaged over the Niño3.4 region (5°N–5°S, 120°–170°W) from in a 100-yr period of the 321-yr long CTRL experiment. Units are in °C. Red lines indicate the ± 0.5 °C threshold for defining ENSO events. Blue lines indicate the standard deviation of Niño3.4 from the NoENSO experiment of ± 0.16 °C

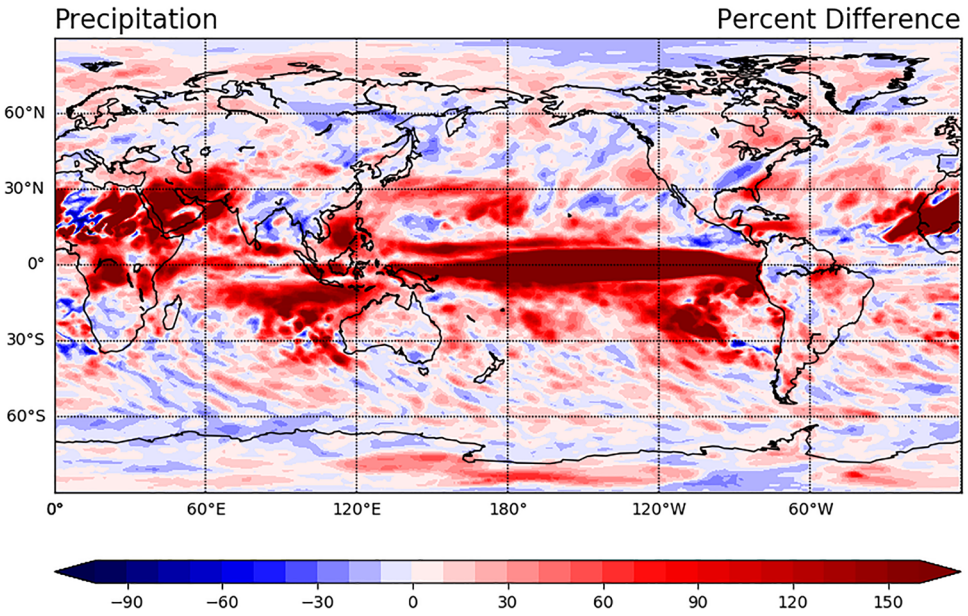

Fig. 3 The percent difference of DJF precipitation variance in the CTRL compared to No ENSO. Red shading indicates the CTRL has more variance

the differences in the other fields shown could be explained by ENSO amplitude asymmetry projecting onto the mean state in the CTRL. Yet if ENSO amplitude asymmetry is to blame, we would expect to see positive skewness in the CTRL Niño3.4 distribution, but that is not the case (see Figure S1). Instead, the origin of the different mean states is due to the asymmetry in the ENSO teleconnection patterns that can possibly be linked to the differing spatial patterns of El Niño and La Niña.

To support the claim that the mean state differences can be linked to ENSO teleconnection asymmetry in the CTRL, Fig. 5 shows the difference in the DJF climatologies between ENSO and ENSO-neutral years from the CTRL experiment. Differences in the climatologies reflect the rectification of ENSO-related asymmetries onto the mean state. The largest SST differences (Fig. 5a) occur in the western Pacific, where differences in El Niño and La Niña spatial patterns occur in this model (cf. Figures S2a and S3a; La Niña patterns stretch farther west). The cool bias in the western Pacific is coupled to reduced precipitation (Fig. 5d), and both the SST and precipitation differences closely mirror the differences shown in the CTRL and NoENSO experiment comparison (Fig. 4a,

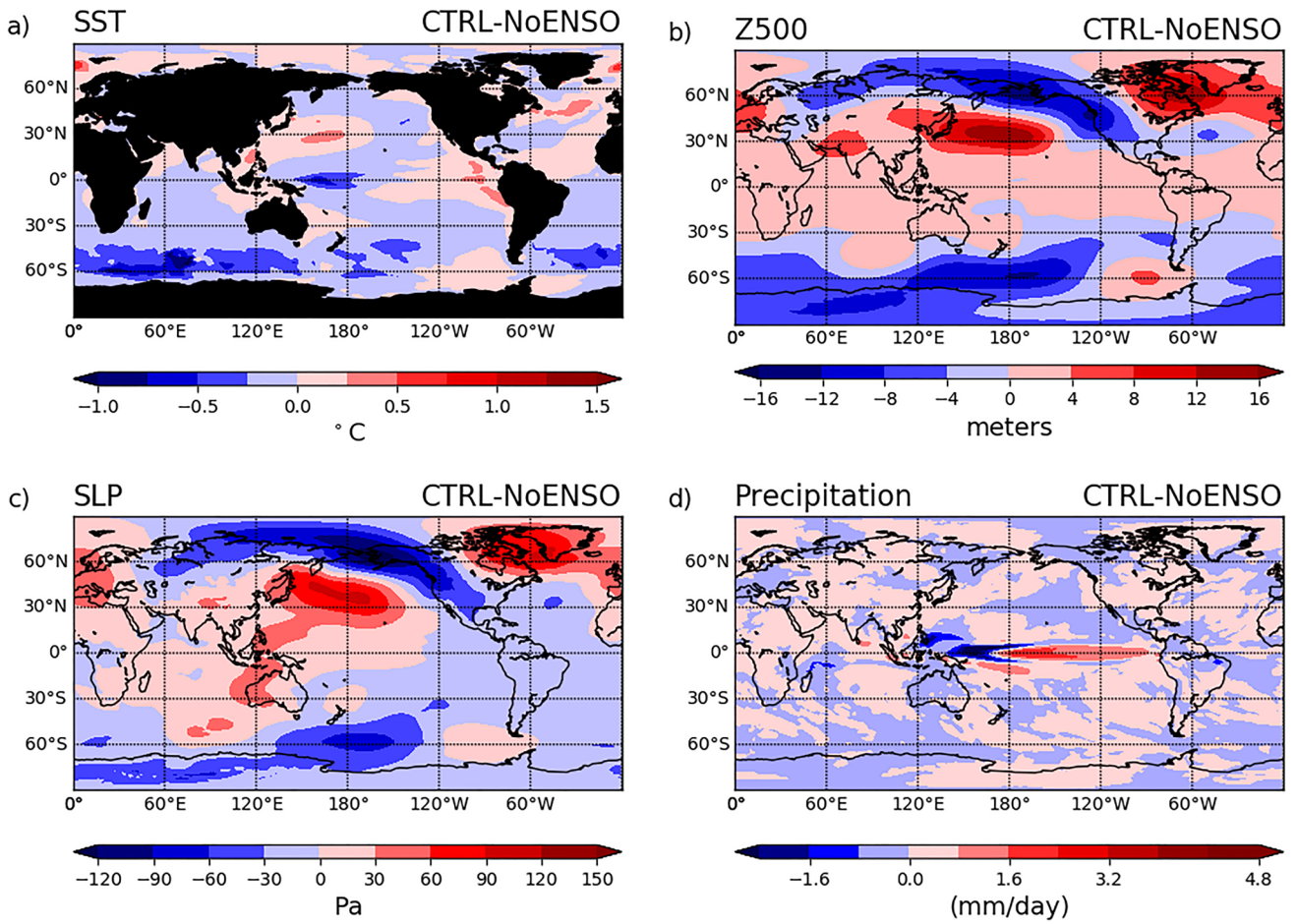

Fig. 4 Difference in CESM1-CAM4 Experiment mean state in DJF (NoENSO – CTRL). **a** sea surface temperature units: °C. **b** 500 hPa Geopotential height units: meters. **c** Sea Level Pressure units: Pascals (**d**) Precipitation units: millimeters per day. Red shading indicates larger values in the CTRL compared to NoENSO

d). The SLP and Z500 mean state differences between the CTRL and NoENSO experiments (Fig. 4b, c) are consistent with the difference between ENSO and neutral years in the CTRL experiment (Fig. 5b, c). This indicates that the mean state bias in the CTRL can be linked to asymmetric ENSO teleconnection patterns, given the consistencies with the separate El Niño and La Niña teleconnection patterns (Figs. S2b-c and S3b-c). For example, if the bias patterns in Fig. 4b, c were due to ENSO amplitude asymmetry, the SLP and Z500 bias patterns should look like a weak El Niño pattern, or positive PNA-like. Instead, the difference patterns exhibit ridging over the North Pacific and troughing over western North America, consistent with the difference in teleconnection patterns associated with El Niño and La Niña in this model (cf. Figures S2b-c and S3b-c).

If the extratropical mean state in the CTRL is biased towards a particular ENSO teleconnection pattern, the calculation of anomalies and subsequent composites of ENSO teleconnections will inherit this bias as well. To circumvent this caveat, we instead compute DJF mid-level atmospheric circulation anomalies, estimated using Z500, from the CTRL based on the NoENSO reference climatology rather than the CTRL reference climatology. These anomalies are then used for the El Niño and La Niña composite maps (Fig. 6 a, b). The Z500 anomalies during El Niño reflect a positive PNA-like pattern, whereas a negative PNA-like pattern is present during La Niña. One can see that the Z500 anomalies across North America, particularly along the U.S. west coast and southeast are stronger during El Niño than during La Niña.

To quantitatively compare the amplitude of the teleconnection anomalies across North America and other latitudes, Fig. 6c shows the latitudinal profiles of Z500 at 96°W (gold line in Fig. 6a, b), which intersect the North American centers of action of the PNA pattern. When El Niño (red) and La Niña (blue) composite anomalies from the CTRL are computed with respect to the unbiased NoENSO reference climatology ("NoENSOref" solid curves), the amplitude asymmetry of the teleconnections becomes more distinct, with El Niño-forced atmospheric circulation anomalies in both hemispheres being larger in

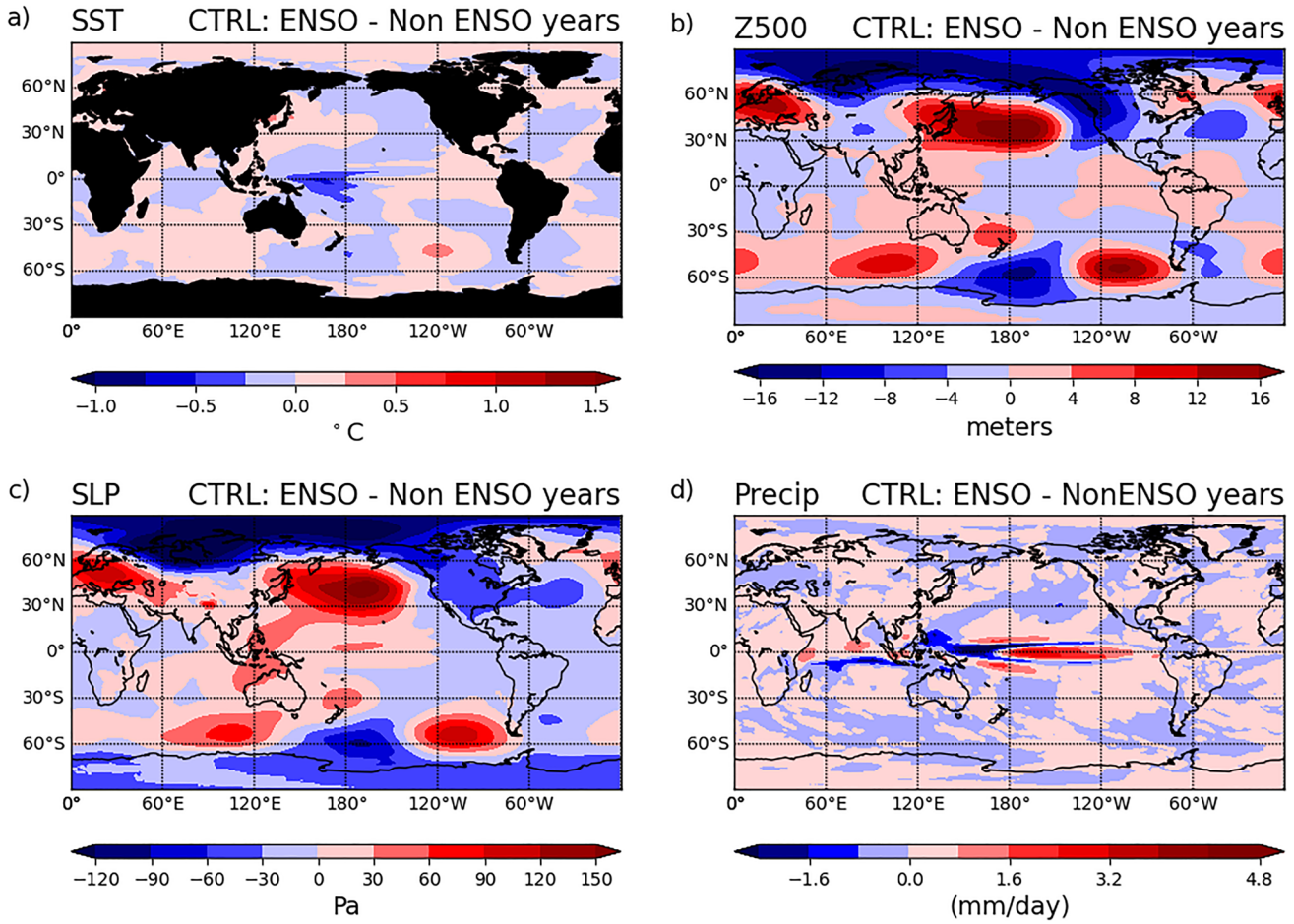

Fig. 5 Difference in CTRL mean state in DJF for ENSO years versus ENSO-neutral years. **a** sea surface temperature units: °C. **b** 500 hPa Geopotential height units: meters. **c** Sea Level Pressure units: Pascals (**d**) Precipitation units: millimeters per day. Red shading indicates larger values during ENSO years versus ENSO-neutral years

magnitude than those driven by La Niña. However, when the anomaly composites are instead computed with respect to the ENSO biased CTRL reference climatology ("CTRL-ref" dashed lines), much of the Z500 asymmetry disappears along this latitude: El Niño teleconnection anomalies weaken and La Niña teleconnection anomalies strengthen, resulting in teleconnections of comparable magnitude at most latitudes. Overall, when the mean state is biased due to asymmetries in ENSO and/or its teleconnections, as in the CTRL, many models, and observations, composite comparisons of ENSO teleconnections will inherit those biases. In the case of our model, this results in an underestimate of the amplitude of El Niño teleconnections and overestimate of the amplitude of La Niña teleconnections across central North America, resulting in an underestimate of the teleconnection asymmetry. We note that using any DJF reference climatology will not change the variance, but the anomaly patterns themselves are clearly sensitive to the chosen reference climatology.

3.3 ENSO impact on atmospheric circulation variability

To show the impact of ENSO on the interannual mid-level atmospheric circulation variability, we analyze and compare the DJF Z500 variance in the CTRL and NoENSO experiments. In both experiments, the largest Z500 variability in DJF occurs in the mid and high latitudes, with largest variance occurring in the North Pacific related to fluctuations in the position and strength of the Aleutian Low (Fig. 7a, b). While the CTRL and NoENSO experiments produce a similar pattern, significant differences in variance are present in both hemispheres and at most latitudes (Fig. 7c). As expected, ENSO enhances variability throughout the tropics, as indicated by the band of significantly increased variance roughly between 20°N-20°S. However, unexpectedly, ENSO reduces interannual variance in several regions, specifically in the extratropics, shown by the regions of blue shading in Fig. 7c. In the extratropics, regions of reduced variability are

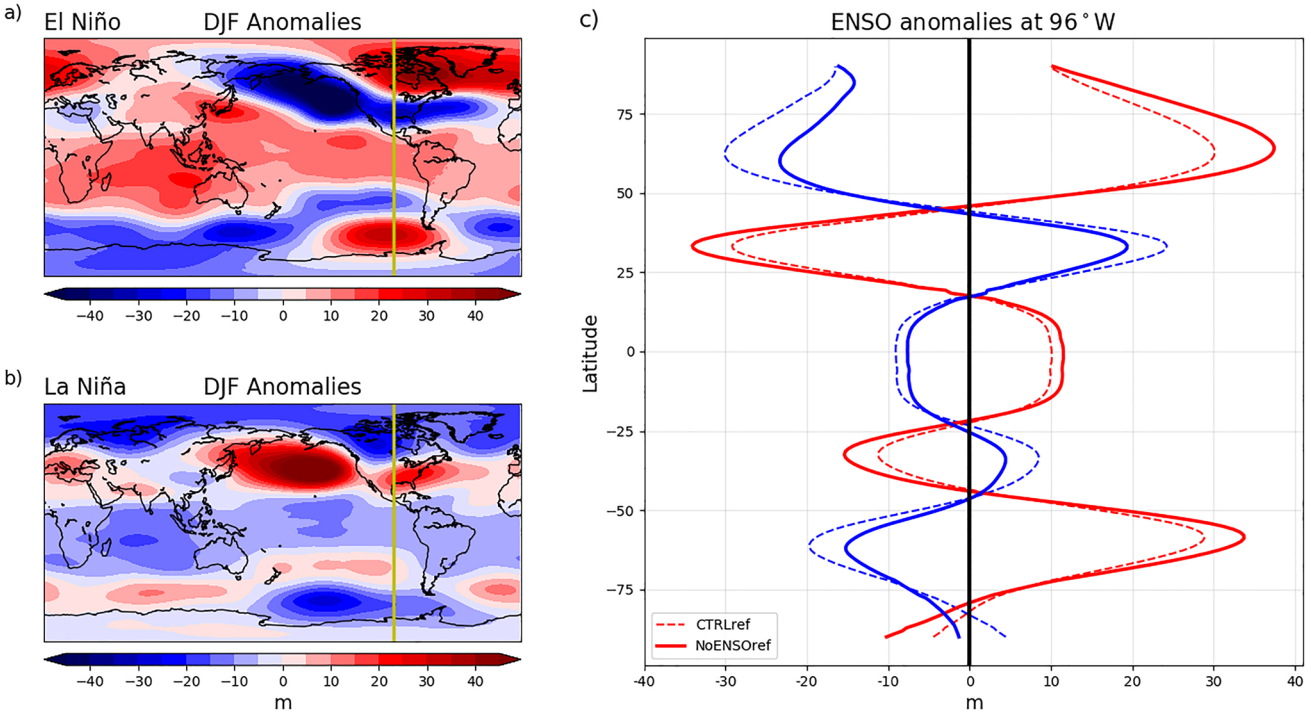

Fig. 6 **a**, **b** DJF Z500 composite anomalies from the CTRL for (top) El Niño and (bottom) La Niña. Anomalies are calculated by removing the DJF climatology from the NoENSO experiment. Units are in meters. Red shading shows higher than average heights and blue shading indicates lower than average heights. **c** Latitudinal profile of DJF Z500 ENSO composite anomalies at 96°W. Red lines: El Niño composite anomalies. Blue lines: La Niña composite anomalies. Solid lines: Anomalies based on the NoENSO reference climatology. Dashed lines: Anomalies based on CTRL reference climatology. Units: meters

often adjacent to the regions of enhanced variability, indicated by a dipole-like structure. This suggests that variability is displaced from one region into another. This is particularly evident over North America, where a large region of enhanced variability is found over the southern U.S., which is located south of the region with strongest reduced variability in the north central U.S. and southern Canada, centered at (45°N, 96°W). Interannual atmospheric circulation variability over this region of North America is the focus of subsequent analyses in this work.

Next, we refer to the ENSO composite anomaly maps from the CTRL (Fig. 6) to aid in interpretation of the changes in Z500 variance. As discussed previously, the strongest ENSO-driven Z500 anomalies are associated with a PNA-like pattern over North America. Notably, Z500 anomalies over North America during both ENSO phases are closely symmetric with respect to their pattern, although not in terms of amplitude. These regions where ENSO drives the largest Z500 anomalies correspond with the three main red shaded regions near North America in Fig. 7c (e.g., where ENSO enhances interannual Z500 variance). The region of displaced variability in North America in Fig. 7c is located where ENSO-driven anomalies are near zero in Fig. 6. To show this more clearly, we return to the latitudinal profile in Fig. 6c. The region of displaced variability is centered around 40°N, where the variance of Z500 anomalies for both El Niño and La Niña are close to zero, whereas the adjacent latitudes show substantially enhanced variability. This suggests that ENSO preferentially drives variability to the north and south, away from the specified region. Therefore, when ENSO-forced variability is absent as in the NoENSO experiment, Z500 variability is not preferentially displaced away from the north central U.S. and southern Canada, resulting in higher local atmospheric variability when compared to the CTRL.

We next determine if similar ENSO-related patterns of enhanced and reduced variability over North America can be derived from the NCEP/NCAR and ERA5 reanalysis products, despite the short record. We note that this is not an apples-to-apples comparison with the model experiments for a number of reasons. First, the amplitude of tropical Pacific SST variability, even when only selecting ENSO-neutral years from reanalysis years, still exhibits larger temperature fluctuations than the NoENSO run. If we had only selected reanalysis years in which Niño3.4 from observations does not exceed the standard deviation of Niño3.4 in the NoENSO experiment (0.16 °C as opposed to the typical 0.5 °C threshold for ENSO-neutral), the sample size would be drastically reduced. Second, instead of using the total variance from all years compared to ENSO-neutral to compute the variance

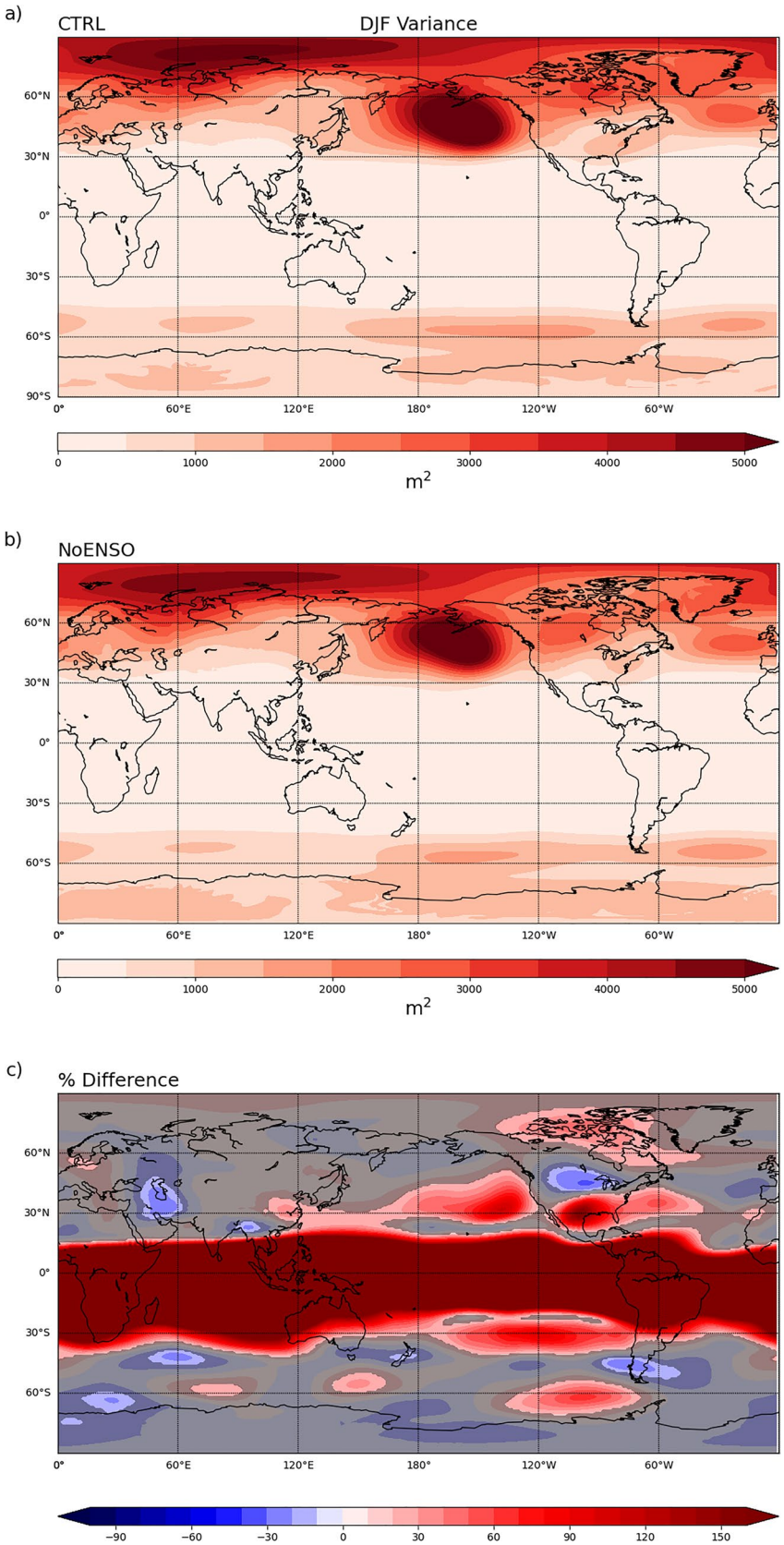

Fig. 7 DJF 500 hPa geopotential height (Z500) variance for **a** the CTRL and **b** the NoENSO experiments. **c** percent difference in DJF Z500 variance between the CTRL and NoENSO. Red shading indicates including ENSO-related variability results in increased variance, whereas blue shading indicates including ENSO-related variability results in reduced variance. Gray transparent shading indicates grid points where the difference is insignificant based on the 95% confidence level

difference, we only use the ENSO years from observations. These modifications increase the possibility that this simple formulation can isolate differences in ENSO-related variance despite the smaller sample size.

Both ERA5 and NCEP/NCAR reanalysis products show regions where ENSO enhances and reduces Z500 variance (Fig. 8). ENSO enhances variability across the global tropics and over parts of North America. Three main regions of enhanced variability over North America are located off the west coast of the U.S., across the southeastern U.S., and in northern Canada. This pattern generally agrees with the model experiment comparison (Fig. 7c), with differences in the spatial extent and amplitude in some regions. Notably, a region of statistically significant reduced variance emerges over the central-western U.S., suggesting that the presence of ENSO forcing and related teleconnections act to reduce variability. Similar to the model experiment comparison, enhanced variance off the west coast of the U.S. and across the southeast are adjacent to the region of reduced variability, indicating that variability typically occurring during ENSO-neutral years is displaced away from the reduced variance region. Notably, the location of the reduced variance region from the reanalysis products is slightly southwest of the model-derived pattern. Deficiencies in model teleconnection patterns, differences in sample size, and differences in the threshold used to define ENSO-Neutral could all potentially explain the differences in the amplitude and spatial patterns between the model derived patterns and that from the reanalysis products. The occurrence of a reduced variance region over North America in the reanalyses is encouraging and suggests the model experiments are likely picking up on physically realistic changes in variability.

To test the sensitivity of the reanalysis results to the ENSO-neutral threshold, we redefine ENSO-neutral years from observations as those when the DJF Niño3.4 does not exceed 0.16 °C in magnitude (to match the typical variability of the NoENSO experiment) and reproduce the percent difference plot (not shown). While the results varied quantitatively, similar spatial patterns emerged from the reanalysis products, suggesting that the results are qualitatively insensitive to the threshold used to define ENSO-neutral. Although, using the stricter threshold also results in a drastic reduction

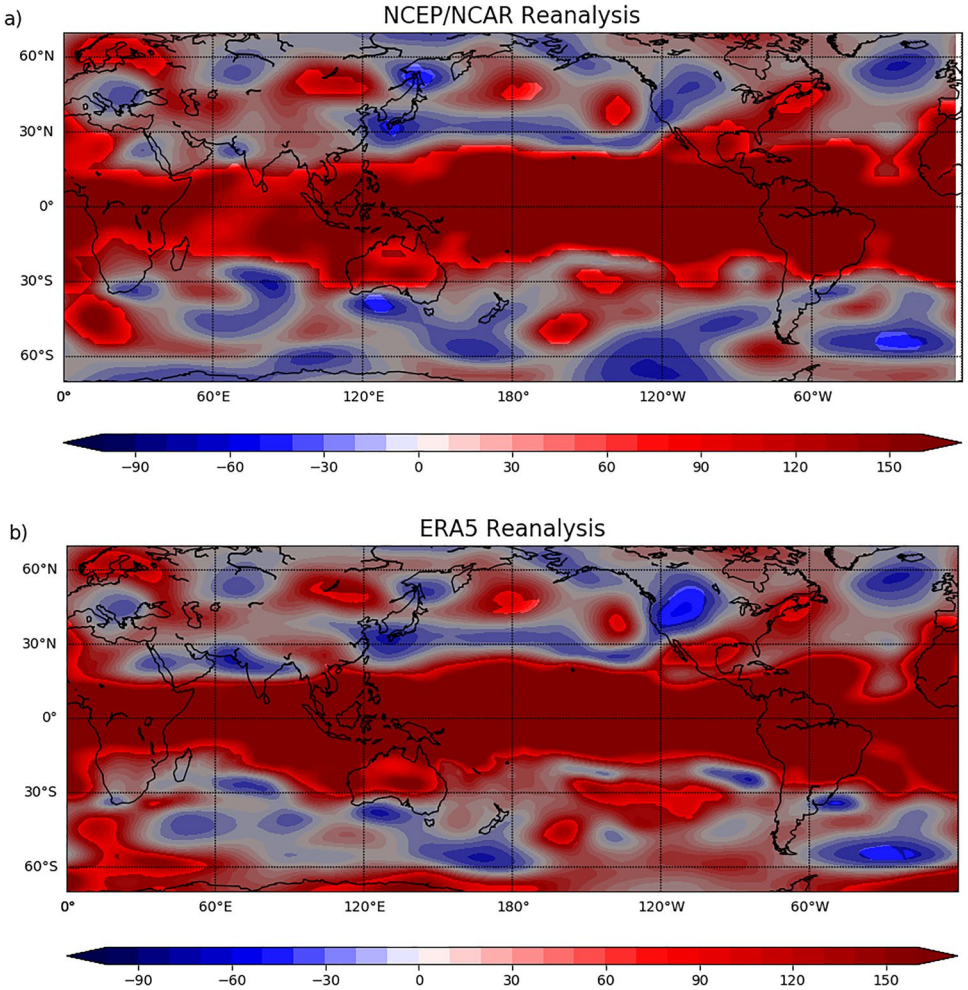

Fig. 8 Percent difference in DJF Z500 variance between observed ENSO and ENSO-neutral years from **a** NCEP/NCAR Reanalysis and **b** ERA5 reanalysis from 1950–2020. ENSO events are defined as meeting or exceeding 0.5 °C Niño3.4 magnitude. Red shading indicates larger variance during ENSO years. Blue shading indicates larger variance during ENSO-neutral years. Grey shading: Insignificant values based on a 90% confidence level

in the number of years that classify as ENSO neutral (5 compared to 26 for the 0.5° threshold) and increase in the number of years that classify as ENSO years (65 compared to 44 for the 0.5° threshold), further clouding the interpretation of results. The insight we can take from this analysis is that the results appear quantitatively sensitive to the number of ENSO-neutral years sampled, thus motivating our approach in the subsequent section. For the remainder of the analyses, we assume that the exact threshold for defining ENSO-neutral is less important than how the threshold chosen impacts the sample size of ENSO-neutral years. We also assume that teleconnection patterns in the model are generally realistic, as shown in Deser et al. (2012) for a pre-industrial version of a similar model, and proceed by exploring the sensitivity of the model results to sampling variability of ENSO-neutral years.

3.4 Sensitivity to ENSO neutral sample size

In this section, we apply Monte Carlo sampling to estimate the sensitivity of the model comparison results (e.g., Fig. 7c) to the sample size of ENSO-neutral years. The goals of this analysis are to quantitatively demonstrate 1) the extent to which the ENSO-forced variance (i.e., as inferred from the percent difference in variance) is sensitive to the number of ENSO-neutral years sampled and 2) how variable results are across same-size random samples of ENSO-neutral years. Together, these measures will allow us to estimate how large a sample size of ENSO-neutral years is necessary to resolve ENSO's forced Z500 response in this model, the results of which are tested in the subsequent section.

For example, say we estimate how ENSO drives a change in Z500 variance by computing the percent difference in variance between the CTRL and NoENSO, but instead restrict the estimate of the Z500 variance from the NoENSO experiment (the non-ENSO variance) to one iteration of 40 randomly sampled ENSO-neutral years. A sample of 40 ENSO-neutral years is chosen because only 40 years from the CTRL exhibit tropical Pacific SST variability as minimal as NoENSO (less than 0.16 °C Niño3.4 magnitude). We then repeat this analysis 8 additional times and display the 9 different estimates of how ENSO changes the Z500 variance in Fig. 9. Notably, the CTRL Z500 variance never changes—only the variance estimated from the NoENSO experiment changes with each iteration. Notice that the amplitude and spatial extent of the increased variance regions vary across iterations. Also, some iterations produce a substantial region of reduced variance over North America while others do not.

Additionally, the enhanced variance over Northern Canada does not emerge in all iterations and varies widely in amplitude across iterations. Overall, the spatial pattern changes with each random sample of non-ENSO variance, suggesting that the resulting variance estimates are dependent on which randomly sampled 40 NoENSO

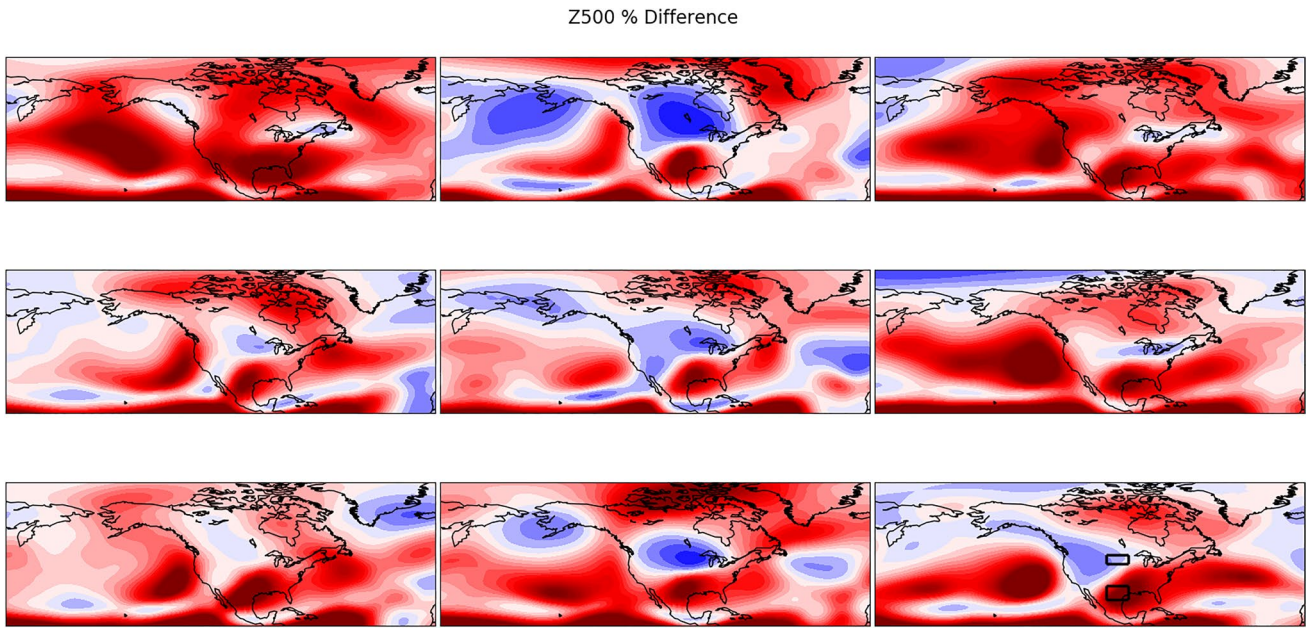

Fig. 9 Example of how sampling variability of ENSO-neutral years impacts the estimate of ENSO-forced changes in Z500 variability. Each panel shows the percent difference in DJF Z500 variance between the CTRL and NoENSO, with the NoENSO sample size restricted to 40 randomly sampled years with replacement. Red shading indicates including ENSO-forced variability results in increased variance. The two regions of focus for Fig. 10 are indicated in the lower right-hand panel. The domains are: southern box (27°N–33°N, 105°W–95°W) and northern box (43°N–47°N, 105°W–95°W)

years are selected. This analysis is then extended to 10,000 total iterations with replacement, meaning that when one year from the NoENSO experiment is selected, it is immediately reintroduced into the population. We apply this Monte Carlo random sampling approach to ENSO-neutral year sample sizes of 20, 40, 60, and up to 300 in intervals of 20 to identify at what sample size the sensitivity begins to diminish. As the sample size approaches 300, the number of possible unique random samples approaches one.

We focus results on two regions (see domains in bottom right panel of Fig. 9): the southeast U.S. (27°N-33°N, 105°W-95°W) where ENSO significantly enhances Z500 variance and the region directly to the north (43°N-47°N, 105°W-95°W) where ENSO displaces variability, resulting in reduced variability during ENSO years, as seen in Fig. 7. The above procedure is modified slightly to display the average percent change in variance across iterations for each sample size, averaged over the specified domains (Fig. 9). The area-weighted average NoENSO variance is calculated at both locations for all 10,000 iterations at each sample size. Then, the ensemble average NoENSO variance is calculated by averaging the area-weighted average variance over all iterations at each sample size. This value is used to calculate the percent difference from the CTRL. The CTRL variance is constant across all sample sizes and is the same estimate used in Fig. 7c.

Figure 10 (top panel) shows the results of the Monte Carlo simulation over the region where ENSO drives a reduction in Z500 variance over North America. The blue dots represent the percent change based on the average NoENSO variance at each sample size. We define the "truth" as the percent change in variance estimated from a 300-yr sample size of ENSO-neutral years from the NoENSO experiment (e.g., the rightmost blue dot). The uncertainty decreases with increasing sample size, as expected. When 300 years of the NoENSO time series are used to estimate the non-ENSO variance, the results show that ENSO drives a 25% reduction in Z500 variance over the Northern United States and Southern Canada. This result is only slightly underestimated at the smallest sample size of 20, with ENSO driving a 21% reduction in Z500 variance, although the uncertainty is large. The large uncertainty at smaller sample sizes suggests that a wide range of results are possible when only a small number of ENSO-neutral states are sampled. For example, when a subset of 20 random neutral years is used, the resulting percent change can range from an increase in variance of roughly 80% to a reduction in variance of about 125%. The average magnitude of the displacement (-25%) is reproduced when roughly 60–80 ENSO neutral years are used in the calculation, although the uncertainty is too large to confidently expect consistent results across different samples. It is not until the sample size increases to 240 ENSO neutral years that the uncertainty drops to within 10% of our "truth" estimate, as shown with the horizontal dashed lines.

Figure 10 (bottom panel) shows the results of the Monte Carlo simulation over the region where ENSO drives an increase in Z500 variance over the southeast U.S. When 300 years are used to estimate the non-ENSO variance, ENSO increases variance in this region by roughly 155%. The average percent change is overestimated at a sample size of 20 years, with ENSO estimated to increase the variance by 165%. The average magnitude of the enhanced variance is reproduced when roughly 120–140 ENSO-neutral years are used, although the uncertainty is large. It is not until the sample size increases to 180 years that the uncertainty drops to within 10% of our "truth" estimate.

Based on findings from both regions, an estimated 240 ENSO neutral years are needed to reduce the sensitivity to sample size. However, some impacts, including the increased variance in the southeast U.S., are reproduced with low uncertainty with as few as 180 ENSO neutral years. The sign of the impacts, whether variance will be enhanced or reduced, may be resolved at smaller sample sizes, but the magnitude is not consistent due to large uncertainty. These results imply that a multi-century simulation length of approximately 1800 model years is needed to obtain 240 ENSO-neutral years and resolve the full impact of ENSO on interannual atmospheric variability in this model, based on the ratio of 260 ENSO to 40 ENSO neutral years (defined as when Niño3.4 magnitude is less than 0.16 °C) obtained from 300 years of the CTRL run.

3.5 Testing the sample size estimate

Finally, the CESM2 model is used to test the hypothesis that if a simulation is sufficiently long to simulate at least 240 ENSO neutral years, sensitivity to sample size will diminish and the impact of ENSO on interannual atmospheric variability, particularly over North America where ENSO appears to displace variability, can be reproduced consistently. To test this hypothesis, the full 2000-yr CESM2 simulation is used. The simulation length surpasses the previously stated 1800 model years needed, but the periodicity of ENSO is different in CESM2 and 2000 model years only affords 195 ENSO-neutral years. ENSO is categorized based on the same definition used above, where an ENSO-neutral year is defined as when the magnitude of SST variability in the CESM2 Niño3.4 region is within the NoENSO standard deviation (0.16 °C). Although 195 is fewer than our estimate based on CESM1-CAM4, the sensitivity analysis suggests that the sign of the percent change in variance should be reproduced with this smaller ENSO neutral sample size, although with some uncertainty in the magnitude. We compute the spatial map of the percent change in variance due

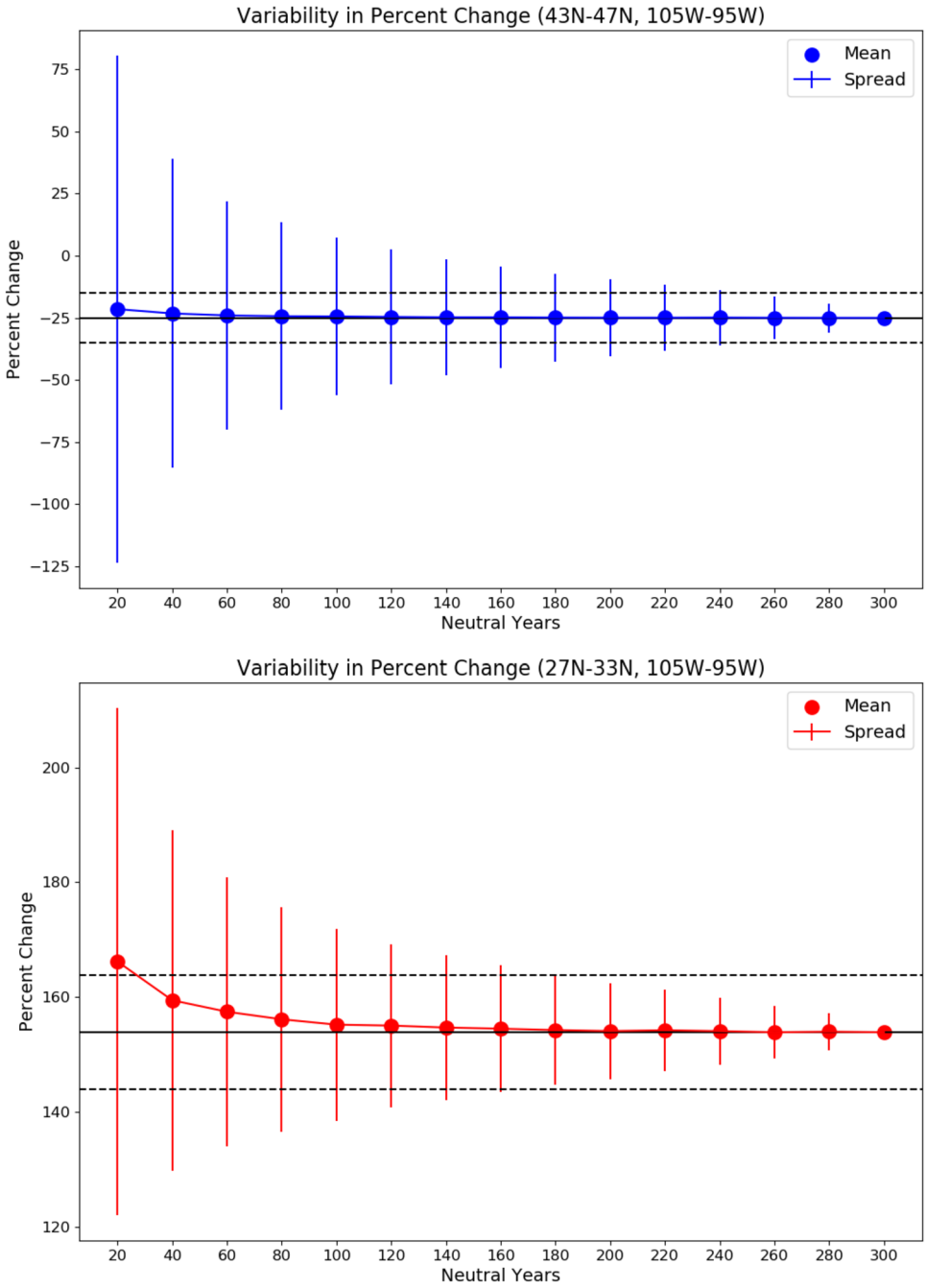

Fig. 10 Sensitivity of the percent change in Z500 variance driven by ENSO to the sample size of ENSO-neutral years for a region in the (bottom panel) southeast U.S. (27°N–33°N, 105°W–95°W) and (top panel) directly to the north (43°N–47°N,105°W–95°W). Bold dots are the percent change based on the average NoENSO variance of a particular sample size, estimated from 10,000 random samples. Error bars are the percent uncertainty in the variance change derived from the standard deviation of individual samples of NoENSO variance at each sample size. The x-axis is sample sizes of ENSO-neutral years. Horizontal dashed lines indicate at what value the uncertainty is 10% of the "truth."

to ENSO (Fig. 11) similar to that in observations, but with a 0.16 °C threshold for ENSO-neutral. A similar spatial pattern as Fig. 7c from the model experiment comparison emerges, with ENSO driving enhanced variability off the west coast of the United States, the southeastern U.S., and northern Canada. A small yet significant region of reduced variability is present over the north central United States and into Canada and is in the same general location as shown in Fig. 7c. The CESM2 results show that ENSO drives a 10–20% reduction in Z500 variance over the Northern United States and Southern Canada, which is well within the uncertainty for a sample size of 200 ENSO neutral years (Fig. 10 top panel).

4 Summary and conclusions

In this study, we investigate the ENSO-driven impact on mid-level atmospheric circulation variability over North America during boreal winter using two coupled model experiments, CTRL and NoENSO. The CTRL contains ENSO variability, whereas in the NoENSO experiment, a

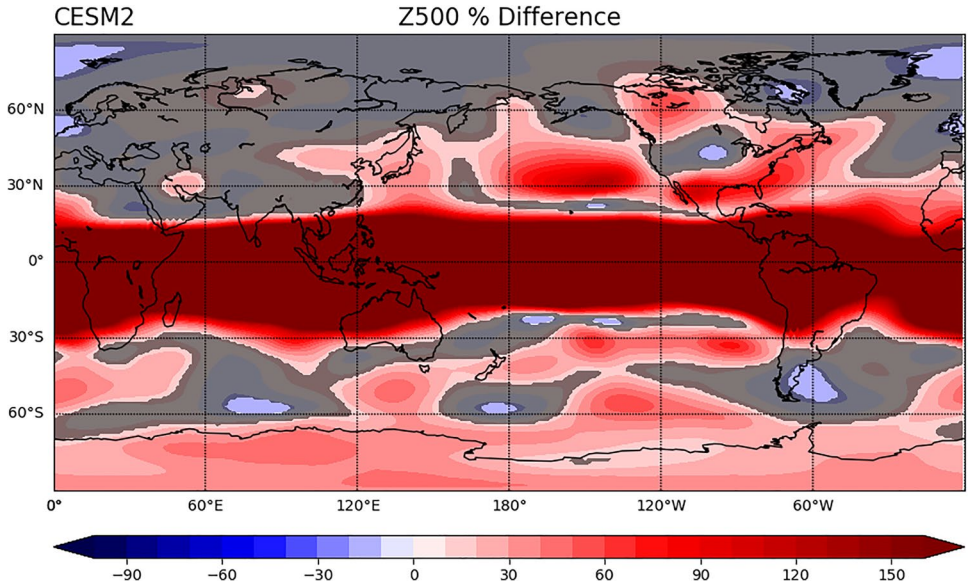

Fig. 11 CESM2 DJF Z500 percent difference in variance. Comparison between CTRL ENSO and Neutral events based on a Niño3.4 ENSO threshold of ±0.16 °C, from the NoENSO Niño3.4 standard deviation. Red shading: ENSO increases variability. Blue shading: ENSO reduces variability. Grey shading: Insignificant values based on a 90% confidence level

novel modeling approach is used to dynamically suppress the Bjerknes feedback, thus eliminating ENSO variability. These model experiments, as well as reanalysis products, are analyzed to address the following three questions and related discussions.

To what extent do asymmetries related to ENSO and/or its teleconnections bias the mean state and impact interpretations of the asymmetry of ENSO teleconnections? To address this question, we use the NoENSO experiment to obtain an unbiased estimate of the seasonally varying climatology in the model. Comparing the DJF mean state between the CTRL and NoENSO experiments reveals that the asymmetry of ENSO teleconnections, possibly linked to different spatial patterns of El Niño and La Niña, projects onto the CTRL mean state. By consequence, when the mean state is biased towards this teleconnection pattern, as in the CTRL (Figs. 4, 5), composite anomalies for ENSO years underestimate the amplitude of El Niño teleconnections and overestimate the amplitude of La Niña teleconnections, resulting in an underestimate of the teleconnection asymmetry (e.g., Fig. 6c). Using the unbiased NoENSO climatology to construct the CTRL ENSO composites reveals that the model produces substantial teleconnection asymmetry, with the magnitude of El Niño-forced Z500 anomalies distinctly stronger than those during La Niña (Fig. 6). As a result, we suspect that ENSO teleconnection asymmetry is generally underestimated in many studies for a variety of reasons, including asymmetries in ENSO itself as well as the asymmetry of ENSO teleconnections, as in our model (Zhang and Sun 2014).

How does ENSO alter mid-level atmospheric circulation variability over North America? Our initial hypothesis was that removing a forcing, such as ENSO, results in reduced variability in the atmospheric circulation where ENSO teleconnections are known to occur and little-to-no change in variance in regions where ENSO's forced signal does not reach. While this topic has been widely studied, we are surprised to conclude that while ENSO enhances Z500 variability in several known regions over North America (e.g., Wallace and Gutzler 1981; Trenberth et al. 1998), ENSO also displaces variability away from north central U.S. and southern Canada, resulting in less variability during ENSO years than during ENSO-neutral years (Fig. 7c). This result is also reproduced in reanalysis products, although the spatial patterns vary slightly. Here we consider both El Niño and La Niña events and their overall impact on Z500 variance, but prior studies argue that El Niño reduces internal variability at 200 hPa over the North Pacific PNA region (Peng and Kumar 2005; Abid et al. 2015; Chapman et al. 2021), whereas La Niña increases variability (Peng and Kumar 2005).

How long of a simulation length is needed to resolve the ENSO-forced change in mid-level atmospheric circulation variability? A Monte Carlo random sampling method is used to determine the total number of ENSO-neutral years needed to consistently obtain the amplitude of the ENSO-forced variance in Z500 within 10% uncertainty. We find general consistency in the mean estimate of the non-ENSO variance over 10,000 random samples for even small sample sizes (20, 40, 60, 80) of ENSO-neutral years, however the uncertainty in the estimate is too large for small sample sizes to have confidence in any single sample (Figs. 9, 10). We find that approximately 240 ENSO-neutral years are needed to estimate the ENSO-forced reduction in variance over the Northern U.S. and southern Canada within 10% uncertainty, thus consistently obtaining the decline in Z500 variance in each individual sample. Over the southeast U.S., where ENSO drives an increase in variance, fewer ENSO-neutral

years are needed—a sample size of approximately 180—to consistently obtain within 10% the increase in Z500 variance in each individual sample. Therefore, roughly 240 ENSO-neutral years are ideal to closely resolve the ENSO forced change in Z500 variance over North America in this model. Using this estimate, we show that a 2000-yr CESM2 simulation with roughly 200 ENSO-neutral years produces a similar pattern of significantly reduced variability during ENSO years (Fig. 11). However, the amplitude of the reduced variance is weaker in CESM2 but within the uncertainty estimated from the CESM1-CAM4 experiments (Fig. 10). We suspect that the amplitude and spatial pattern of the reduced variance varies across long simulations from other models. Many previous studies have addressed the limitations of exclusively using observational datasets to investigate the ENSO forced response (Wittenberg 2009; Stevenson et al. 2010; Deser et al. 2017, 2018). These studies find that the majority of uncertainty in the ENSO-forced response found in observations is the result of large internal atmospheric variability. Stevenson et al. (2010) concluded that a simulation length of a minimum of 250 years is needed to obtain stable ENSO statistics. Based on results found in the present study, a minimum simulation length of at least 1800 years is needed to consistently estimate the ENSO-forced variance. While this estimate is strictly based on CESM1-CAM4 ENSO behavior, we note that this estimate is an order of magnitude larger than previous suggestions.

There are a few limitations to the results presented in this work. Although CESM1-CAM4 has proven adequate in simulating ENSO and ENSO teleconnections, limitations still exist in the model's ability to replicate the observed frequency and amplitude of ENSO events. For example, if the ratio of ENSO-neutral to ENSO years is higher in a particular model than what is found in CESM1-CAM4, then a simulation length of less than 1800 years may be adequate to resolve the non-ENSO variance. We expect the total number of simulation years necessary to resolve ENSO-forced changes in variance depends on the ENSO statistics of a given model. If the amplitude of SST variability in the equatorial Pacific is overestimated, as in CESM1-CAM4, this could impact the strength of the teleconnected response and overestimate the amplitude of ENSO-forced variability found over North America. A weaker ENSO signal then could require a larger sample of ENSO years for the signal to rise above the internal variability.

We also acknowledge that the ability to utilize the model experiments in this study to investigate ENSO's impact on a more regional and finer temporal scale is limited by the resolution of the CESM1-CAM4 and data availability. ENSO has been shown to influence the seasonal probability distribution functions (PDFs) of precipitation and temperature on daily scales, particularly on the frequency of daily extreme events found in the tails of the PDFs (Gershunov 1998; Cayan et al. 1999). Daily data was not stored for the CESM1-CAM4 experiments, however the rich CESM2 archive could offer an opportunity to extend this analysis to regional terrestrial impacts on shorter timescales.

Supplementary Information The online version contains supplementary material available at https://doi.org/10.1007/s00382-023-07058-1.

Acknowledgements M.S. thanks Drs. Walt Robinson and Anantha Aiyyer for helpful comments and suggestions on an earlier version of this work. S.M.L thanks Mahdi Hasan for generating Supplementary Figure S1 and discussions related to ENSO amplitude asymmetry in the CESM1-CAM4 model. We also acknowledge computation support from the NCSU HPC services.

Authors contributions All authors contributed to the study conception and design. S.L performed model experiments and M.S. performed data analysis. The first draft of the manuscript was written by M.S. and all authors commented on and wrote sections in subsequent versions of the manuscript. All authors read and approved the final manuscript.

Funding This work was supported through NSF Grant AGS-2223262.

Data availability CESM2 FCM output is available from the Earth System Grid Federation (ESGF; at http://esgf-node.llnl.gov/search/cmip6). CESM1-CAM4 simulations were run by the authors, and output is available upon request. ERA5 datasets were obtained freely from Copernicus Climate Change Service at https://doi.org/https://doi.org/10.24381/cds.f17050d7. NCEP-NCAR Reanalysis 1 data is provided by the NOAA PSL, Boulder, Colorado, USA, from their website at https://psl.noaa.gov. ERSSTv5 data provided by NOAA's National Center for Environmental Information at their website https://www.ncei.noaa.gov/products/extended-reconstructed-sst.

Declarations

Conflict of interest The author declare that they have no conflict of interest.

Ethical approval Not applicable.

References

Abid MA, Kang I-S, Almazroui M, Kucharski F (2015) Contribution of synoptic transients to the potential predictability of pna circulation anomalies: el niño versus la niña. J Clim 28:8347–8362. https://doi.org/10.1175/JCLI-D-14-00497.1

Alexander MA, Bladé I, Newman M, Lanzante JR, Lau N-C, Scott JD (2002) The atmospheric bridge: the influence of enso teleconnections on air-sea interaction over the global oceans. J Clim 15:2205–2231. https://doi.org/10.1175/1520-0442(2002)015%3c2205:TABTIO%3e2.0.CO;2

An S-I, Jin F-F (2004) Nonlinearity and asymmetry of enso. J Clim 17:2399–2412. https://doi.org/10.1175/1520-0442(2004)017%3c2399:NAAOE%3e2.0.CO;2

Bjerknes J (1969) ATMOSPHERIC teleconnections from the equatorial pacific. Mon Weather Rev 97:163–172. https://doi.org/10.1175/1520-0493(1969)097%3c0163:ATFTEP%3e2.3.CO;2

Bogenschutz PA, Gettelman A, Hannay C, Larson VE, Neale RB, Craig C, Chen C-C (2018) The path to cam6: coupled simulations with cam5.4 and cam5.5. Geoscientific Model Development 11:235–255. https://doi.org/10.5194/gmd-11-235-2018

Capotondi A, Deser C, Phillips AS, Okumura Y, Larson SM (2020) ENSO and Pacific Decadal Variability in the Community Earth System Model Version 2. J Adv Model Earth Syst. https://doi.org/10.1029/2019MS002022

Cayan DR, Redmond KT, Riddle LG (1999) ENSO and hydrologic extremes in the Western United States. J Clim 12:2881–2893. https://doi.org/10.1175/1520-0442(1999)012%3c2881:EAHEIT%3e2.0.CO;2

Chapman WE, Subramanian AC, Xie S-P, Sierks MD, Ralph FM, Kamae Y (2021) Monthly modulations of ENSO teleconnections: implications for potential predictability in North America. J Clim 34:5899–5921. https://doi.org/10.1175/JCLI-D-20-0391.1

Compo GP, Sardeshmukh PD (2010) Removing ENSO-related variations from the climate record. J Clim 23:1957–1978. https://doi.org/10.1175/2009JCLI2735.1

Danabasoglu G et al (2020) The Community Earth System Model Version 2 (CESM2). Journal of Advances in Modeling Earth Systems. https://doi.org/10.1029/2019MS001916

Deser C et al (2012) ENSO and pacific decadal variability in the community climate system model version 4. J Clim 25:2622–2651. https://doi.org/10.1175/JCLI-D-11-00301.1

Deser I, Simpson R, McKinnon KA, Phillips AS (2017) The Northern hemisphere extratropical atmospheric circulation response to ENSO: how well do we know it and how do we evaluate models accordingly? J Clim 30:5059–5082. https://doi.org/10.1175/JCLI-D-16-0844.1

Deser I, Simpson R, McKinnon KA, Phillips AS (2018) How well do we know ENSO's climate impacts over North America, and how do we evaluate models accordingly? J Clim 31:4991–5014. https://doi.org/10.1175/JCLI-D-17-0783.1

Dilley M, Heyman BN (1995) ENSO and disaster: droughts, floods and el Niño/southern oscillation warm events. Disasters 19:181–193. https://doi.org/10.1111/j.1467-7717.1995.tb00338.x

Eyring, V., S. Bony, G. A. Meehl, C. A. Senior, B. Stevens, R. J. Stouffer, and K. E. Taylor, 2016: Overview of the Coupled Model Intercomparison Project Phase 6 (CMIP6) experimental design and organization. *Geoscientific Model Development (Online)*, **9**.

Frauen C, Dommenget D, Tyrrell N, Rezny M, Wales S (2014) Analysis of the nonlinearity of el Niño-southern oscillation teleconnections. J Climate 27:6225–6244. https://doi.org/10.1175/JCLI-D-13-00757.1

Gent PR, Coauthors, (2011) The community climate system model version 4. J Clim 24:4973–4991. https://doi.org/10.1175/2011JCLI4083.1

Gershunov A (1998) ENSO Influence on intraseasonal extreme rainfall and temperature frequencies in the contiguous United States: implications for long-range predictability. J Clim 11:3192–3203. https://doi.org/10.1175/1520-0442(1998)011%3c3192:EIOIER%3e2.0.CO;2

Gill AE (1980) Some simple solutions for heat-induced tropical circulation. Q J R Meteorol Soc 106:447–462. https://doi.org/10.1002/qj.49710644905

Harrison DE, Larkin NK (1998) Seasonal U.S. temperature and precipitation anomalies associated with el niño: historical results and comparison with 1997–98. Geophys Res Lett 25:3959–3962. https://doi.org/10.1029/1998GL900061

Henderson SA, Vimont DJ, Newman M (2020) The critical role of non-normality in partitioning tropical and extratropical contributions to PNA growth. J Clim 33:6273–6295. https://doi.org/10.1175/JCLI-D-19-0555.1

Hersbach, H., B. Bell, P. Berrisford, and coauthors, 2020: The ERA5 global reanalysis - Hersbach - 2020 - Quarterly Journal of the Royal Meteorological Society - Wiley Online Library. https://rmets.onlinelibrary.wiley.com/doi/full/https://doi.org/10.1002/qj.3803 (Accessed July 19, 2021).

Hoerling MP, Kumar A (2002) Atmospheric response patterns associated with tropical forcing. J Clim 15:2184–2203. https://doi.org/10.1175/1520-0442(2002)015%3c2184:ARPAWT%3e2.0.CO;2

Hoerling MP, Kumar A, Zhong M (1997) El Niño, La Niña, and the nonlinearity of their teleconnections. J Clim 10:1769–1786. https://doi.org/10.1175/1520-0442(1997)010%3c1769:ENOLNA%3e2.0.CO;2

Hoskins BJ, Karoly DJ (1981) The steady linear response of a spherical atmosphere to thermal and orographic forcing. J Atmos Sci 38:1179–1196. https://doi.org/10.1175/1520-0469(1981)038%3c1179:TSLROA%3e2.0.CO;2

Huang B et al (2017) Extended reconstructed sea surface temperature, version 5 (ERSSTv5): upgrades, validations, and intercomparisons. J Clim 30:8179–8205. https://doi.org/10.1175/JCLI-D-16-0836.1

Hurrell, J. W., M. M. Holland, P. R. Gent, S. Ghan, J. E. Kay, and P. J. Kushner, 2013: The Community Earth System Model. 22.

Johnson NC, Feldstein SB (2010) The continuum of north pacific sea level pressure patterns: intraseasonal, interannual, and interdecadal variability. J Clim 23:851–867. https://doi.org/10.1175/2009JCLI3099.1

Kalnay E et al (1996) The NCEP/NCAR 40-year reanalysis project. Bull Am Meteor Soc 77:437–472. https://doi.org/10.1175/1520-0477(1996)077%3c0437:TNYRP%3e2.0.CO;2

Kumar A, Chen M (2017) What is the variability in US west coast winter precipitation during strong El Niño events? Clim Dyn 49:2789–2802. https://doi.org/10.1007/s00382-016-3485-9

L'Heureux ML et al (2017) Observing and predicting the 2015/16 El Niño. Bull Am Meteor Soc 98:1363–1382. https://doi.org/10.1175/BAMS-D-16-0009.1

Larson SM, Kirtman BP (2015) Revisiting ENSO coupled instability theory and SST error growth in a fully coupled model. J Clim 28:4724–4742. https://doi.org/10.1175/JCLI-D-14-00731.1

Larson SM, Pegion KV, Kirtman BP (2018a) The south pacific meridional mode as a thermally driven source of ENSO amplitude modulation and uncertainty. J Clim 31:5127–5145. https://doi.org/10.1175/JCLI-D-17-0722.1

Larson SM, Vimont DJ, Clement AC, Kirtman BP (2018b) How momentum coupling affects SST variance and large-scale pacific climate variability in CESM. J Clim 31:2927–2944. https://doi.org/10.1175/JCLI-D-17-0645.1

Larson SM, Okumura Y, Bellomo K, Breeden ML (2022) Destructive interference of ENSO on North Pacific SST and North American precipitation associated with Aleutian low variability. J Clim 1:1–63. https://doi.org/10.1175/JCLI-D-21-0560.1

Lau N-C, Nath MJ (1994) A modeling study of the relative roles of tropical and extratropical sst anomalies in the variability of the global atmosphere-ocean system. J Clim 7:1184–1207. https://doi.org/10.1175/1520-0442(1994)007%3c1184:AMSOTR%3e2.0.CO;2

Li X, Hu Z-Z, Liang P, Zhu J (2019) Contrastive influence of ENSO and PNA on variability and predictability of North American Winter precipitation. J Clim 32:6271–6284. https://doi.org/10.1175/JCLI-D-19-0033.1

Liu Z, Alexander M (2007) Atmospheric bridge, oceanic tunnel, and global climatic teleconnections. Rev Geophys. https://doi.org/10.1029/2005RG000172

Livezey RE, Mo KC (1987) Tropical-extratropical teleconnections during the northern hemisphere winter. part ii: relationships between monthly mean northern hemisphere circulation patterns and proxies for tropical convection. Mon Weather Rev 115:3115–3132. https://doi.org/10.1175/1520-0493(1987)115%3c3115:TETDTN%3e2.0.CO;2

McMonigal K, Larson SM (2022) ENSO explains the link between Indian ocean dipole and meridional ocean heat transport. Geophys Res Lett. https://doi.org/10.1029/2021GL095796

McPhaden MJ, Zebiak SE, Glantz MH (2006) ENSO as an integrating concept in earth science. Science 314:1740–1745. https://doi.org/10.1126/science.1132588

Neale RB, Richter J, Park S, Lauritzen PH, Vavrus SJ, Rasch PJ, Zhang M (2013) The mean climate of the community atmosphere model (CAM4) in forced SST and fully coupled experiments. J Clim 26:5150–5168. https://doi.org/10.1175/JCLI-D-12-00236.1

Newman M, Sardeshmukh PD, Penland C (2009) How important is air-sea coupling in enso and mjo evolution? J Clim 22:2958–2977. https://doi.org/10.1175/2008JCLI2659.1

Peng P, Kumar A (2005) A large ensemble analysis of the influence of tropical ssts on seasonal atmospheric variability. J Clim 18:1068–1085. https://doi.org/10.1175/JCLI-3314.1

Peng P, Kumar A, Hu ZZ (2018) What drove the pacific and north america climate anomalies in winter 2014/15? Clim Dyn 51:2667–2679

Peng P, Kumar A, Chen M, Hu ZZ, Jha B (2019) Was the north American extreme climate in winter 2013/14 a sst forced response? Clim Dyn 52:3099–3110

Ropelewski CF, Halpert MS (1986) North American precipitation and temperature patterns associated with the el niño/southern oscillation (ENSO). Mon Weather Rev 114:2352–2362. https://doi.org/10.1175/1520-0493(1986)114%3c2352:NAPATP%3e2.0.CO;2

Ropelewski CF, Halpert MS (1987) Global and regional scale precipitation patterns associated with the El Niño/southern oscillation. Mon Weather Rev 115:1606–1626. https://doi.org/10.1175/1520-0493(1987)115%3c1606:GARSPP%3e2.0.CO;2

Sardeshmukh PD, Hoskins BJ (1988) The generation of global rotational flow by steady idealized tropical divergence. J Atmos Sci 45:1228–1251. https://doi.org/10.1175/1520-0469(1988)045%3c1228:TGOGRF%3e2.0.CO;2

Smith, R., and Coauthors, 2010: The Parallel Ocean Program (POP) Reference Manual. 141.

Stevenson S, Fox-Kemper B, Jochum M, Rajagopalan B, Yeager SG (2010) ENSO model validation using wavelet probability analysis. J Clim 23:5540–5547. https://doi.org/10.1175/2010JCLI3609.1

Straus DM, Shukla J (2002) Does Enso force the pna? J Clim 15:2340–2358. https://doi.org/10.1175/1520-0442(2002)015%3c2340:DEFTP%3e2.0.CO;2

Stuecker MF, Timmermann A, Jin F-F, McGregor S, Ren H-L (2013) a combination mode of the annual cycle and the el Niño/southern oscillation. Nature Geosci 6:540–544. https://doi.org/10.1038/ngeo1826

Su H, Neelin JD, Meyerson JE (2005) Mechanisms for lagged atmospheric response to ENSO SST forcing. J Clim 18:4195–4215. https://doi.org/10.1175/JCLI3514.1

Trenberth KE, Branstator GW, Karoly D, Kumar A, Lau N-C, Ropelewski C (1998) Progress during TOGA in understanding and modeling global teleconnections associated with tropical sea surface temperatures. Journal of Geophysical Research: Oceans 103:14291–14324. https://doi.org/10.1029/97JC01444

Wallace JM, Gutzler DS (1981) Teleconnections in the geopotential height field during the Northern Hemisphere winter. Mon Weather Rev 109:784–812. https://doi.org/10.1175/1520-0493(1981)109%3c0784:TITGHF%3e2.0.CO;2

Wittenberg AT (2009) Are historical records sufficient to constrain ENSO simulations? Geophys Res Lett. https://doi.org/10.1029/2009GL038710

Wittenberg AT, Rosati A, Delworth TL, Vecchi GA, Zeng F (2014) ENSO modulation: is it decadally predictable? J Clim 27:2667–2681. https://doi.org/10.1175/JCLI-D-13-00577.1

Worley, P. H., A. A. Mirin, A. P. Craig, M. A. Taylor, J. M. Dennis, and M. Vertenstein, 2011: Performance of the Community Earth System Model. *SC '11: Proceedings of 2011 International Conference for High Performance Computing, Networking, Storage and Analysis*, SC '11: Proceedings of 2011 International Conference for High Performance Computing, Networking, Storage and Analysis, 1–11.

Zhang T, Sun D-Z (2014) ENSO asymmetry in CMIP5 models. J Clim 27:4070–4093. https://doi.org/10.1175/JCLI-D-13-00454.1